Scaling Electric Machines to a Megawatt and Material Options

Andrew A. Woodworth,[1] William R. Sixel,[2] Tiffany S. Williams,[3] Witold K. Fuchs,[4] Marisabel Kelly,[5] Diana Santiago,[6] Kristina M. Vailonis,[7] and Evan J. Pineda[8]
NASA Glenn Research Center, Cleveland, Ohio, 44135

Baochau N. Nguyen[9]
Universities Space Research Association, Cleveland, Ohio, 44135

Paria Naghipour[10]
HX5 LLC, Brook Park, Ohio, 44142

Megawatt (MW) electric aircraft propulsion (EAP) is seen as a significant contributor toward achieving the goals set forth by the Sustainable Flight National Partnership. A large part of enabling MW EAP is developing specific-power-dense electric machines. As specific-power-dense electric machines are scaled up from kW to MW power levels, the thermal stresses on the machines increase in both magnitude and performance-affecting characteristics. This is particularly true for the stators of these machines. Analysis via thermal resistance network modeling and multiscale modeling reveals that increasing amounts of heat will be trapped in the stator windings as the power levels increase. The challenges this presents can be addressed through material advancements whereby materials gain multifunctionality. Specifically, the electrical insulation and potting materials, along with the electrical conductor, that compose the stator slot must work together (gain multifunctionality) to relieve the increased thermal stress. Materials research at the NASA Glenn Research Center points to some useful solutions in this trade space.

I. Nomenclature

AWG	=	American Wire Gauge
BNNS	=	boron nitride nanosheets
DMAc	=	dimethylacetamide
DWHX	=	direct winding heat exchanger
EAP	=	electric aircraft propulsion
ε	=	emissivity

[1] Hybrid Electric Aircraft Materials Technical Lead, Materials Chemistry and Physics Branch/Materials and Structures Division, AIAA Member.
[2] Aerospace Engineer, Thermal Systems and Transport Processes Branch/Propulsion Division, nonmember.
[3] Research Chemical Engineer, Materials Chemistry and Physics Branch/Materials and Structures Division, nonmember.
[4] Research Materials Engineer, Materials Chemistry and Physics Branch/Materials and Structures Division, nonmember.
[5] Research Chemical Engineer, Materials Chemistry and Physics Branch/Materials and Structures Division, nonmember.
[6] Research Materials Engineer, Materials Chemistry and Physics Branch/Materials and Structures Division, nonmember.
[7] Research Materials Engineer, Materials Chemistry and Physics Branch/Materials and Structures Division, nonmember.
[8] Research Associate, Multiscale and Multiphysics Modeling Branch, AIAA Member.
[9] Senior Scientist, nonmember.
[10] Research Associate, AIAA Member.

FEM	=	finite element model
FS	=	force spinning
FTIR	=	Fourier transform infrared
h	=	convection coefficient
hBN	=	hexagonal boron nitride
HEMM	=	High Efficiency Megawatt Motor
HFGMC	=	high-fidelity generalized method of cells
K_x	=	thermal conductivity (x is the material or material system that K is describing)
$K_{1,2,3}$	=	directional thermal conductivity
kW	=	kilowatt
MW	=	megawatt
NASA	=	National Aeronautics and Space Administration
NASMAT	=	NASA Multiscale Analysis Tool
PD	=	partial discharge
PDC	=	polymer-derived ceramics
PPSU	=	polyphenylsulfone
PVP	=	polyvinylpyrrolidone
R	=	electrical resistivity
RUC	=	repeating unit cell
ρ	=	density
S	=	surface area
σ	=	Stefan-Boltzmann constant
T	=	temperature
TEAM	=	thermal, electrical, ambient, and mechanical
UIUC	=	University of Illinois Urbana-Champaign
UW	=	University of Wisconsin
V	=	volume

II. Introduction

Megawatt- (MW-) scale electric aircraft propulsion (EAP) continues to be a promising technology for increasing aircraft efficiency to meet 2050 goals set forth by the Sustainable Flight National Partnership [1]. Megawatt-scale EAP requires power-dense MW electric machines (motors and generators) [2]. However, even efficient power-dense motors will produce tens of kilowatts of heat. Most of the heat is created by joule heating in the stator windings, which contain a significant amount of electrical insulation, which is a poor thermal conductor. The cooling of electric machines is therefore a key component to enabling MW-scale applications. Direct cooling of machines uses dielectric fluids that are poor thermal fluids. Water-based fluids offer better thermal characteristics but are poor dielectric fluids (are partially conductive and/or have low breakdown strength), which relegates them to outer cooling jackets or dedicated cooling channels. Complicating the landscape are two different common manners in which a stator can be constructed. Distributed winding patterns (Fig. 1(a)) are used to reduce electromagnetic losses but usually have large end windings that reduce the benefit of the winding pattern. This configuration is often a good candidate for direct cooling. Concentrated winding patterns (Fig. 1(b)) usually have smaller end windings and stator teeth but create more losses elsewhere in the motor system as compared with distributed windings. The concentrated winding configuration is a better candidate for water-cooling jackets or integrated cooling channels, such as direct-winding heat exchanger concepts (DWHXs) [3].

This paper discusses sensitivity of concentrated winding and distributed winding schemes to thermal conductivity of their constituent materials as a function of the scale of the machine. The paper also examines a multiscale model of heat flow from the inside of a Litz wire to a possible heat sink and discusses material solutions under development at the NASA Glenn Research Center that will help enable MW-power-dense electric machines.

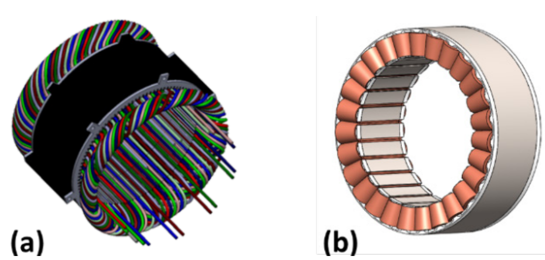

Fig. 1 (a) Distributed windings. (b) Concentrated windings.

III. Results and Discussion

A. Models

1. Thermal Resistance Network Model

When scaling the rated power of electric machines from tens of kilowatts (kW) to the MW scale, one of three paths is usually taken: a) increasing the geometric size (rotor diameter and active length), b) increasing the rotational speed, or c) increasing the electric loading of the machine (which is likely to decrease the efficiency of the machine). The EAP application requirements call for efficient, slower rotating machines; otherwise, a speed-reducing gear box and/or increased thermal system size will be needed, adding weight and complexity. Thus, the thermal network model will examine the impacts of thermal resistance of different components as a function of rotor diameter. A schematic of the slot arrangement that the thermal network model is built upon is shown in Fig. 2. In the network model for the direct windings, there is only one thermal path from the heat generation in the winding to the coolant, whereas for the concentrated windings, the heat transfers through both the back iron and the stator iron (the stator teeth), forming multiple thermal paths.

For points of comparison, here are three developmental high-power-density motors for which specifications have been published:

1. The High Efficiency Megawatt Motor (HEMM, 16 kW/kg, 1.42 MW, 300-mm rotor outer diameter) is a distributed-winding motor developed by NASA [4].
2. Another distributed-winding motor, an outer-rotor machine, is under development at the University Illinois Urbana Champaign (UIUC) (13.8 kW/kg, 1 MW, 263-mm rotor inner diameter) [5].
3. A team at The University of Wisconsin (UW) has been developing a double-layer concentrated-winding machine (23.7 kW/kg, 1 MW, 191-mm outer rotor diameter) [6].

The first thermal model presented (Fig. 2(a)) is for a directly cooled Litz wire, airgap/distributed winding similar to HEMM. The second thermal model presented (Fig. 2(b)) is for an indirectly water-jacket cooled, double-layer concentrated-winding stator like the UW machine. Although the design space is much wider, and several parameters may be changed that can influence the results, this model is designed solely to isolate the impacts of the materials on the system.

Both thermal models rely on several common assumptions about the scaling of electric machines. First, the number of slots and poles is held constant. The remaining dimensions are scaled in proportion to rotor diameter to keep electromagnetic flux constant. These include slot width, tooth width, and back iron thickness. Electric loading is also kept constant (winding current density, A/mm^2). As a result of these assumptions, the rated power of the machine is related to the square of rotor diameter. The distributed-winding machine geometry is scaled based on HEMM, and the concentrated-winding machine geometry is scaled based on the machine described in [7].

In the directly cooled distributed-winding machine, the winding effective thermal conductivity is assumed to be 3 $W/m \cdot K$. For the concentrated-winding machine, it is assumed to be 4 $W/m \cdot K$, because an epoxy with higher thermal conductivity can be used. For this model, the effective winding thermal conductivities are an amalgam of conductor, insulator, and potting material; are perpendicular to the Litz wire; and have been measured [8] or calculated [9]. In the double-layer concentrated-winding machine, the winding effective thermal conductivity is calculated using a homogenization method [10]. In both machines, the slot liner thickness is assumed to be 0.18 mm (0.007 in.) and its thermal conductivity equal to 0.1 $W/m \cdot K$. The stator iron thermal conductivity is assumed to be 27 $W/m \cdot K$. The direct-cooled machine is assumed to have 108 slots and a convection coefficient of 1000 $W/m^2 \cdot K$. The water-jacket-cooled

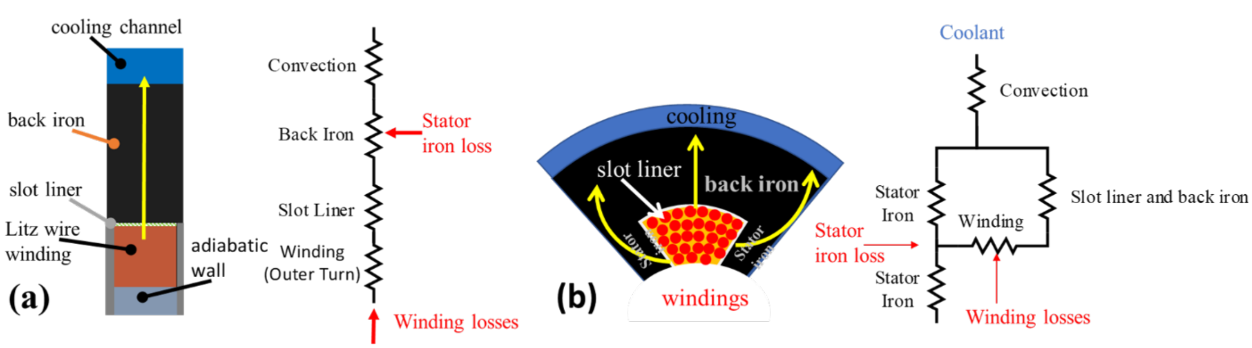

Fig. 2 Schematic and thermal resistance network for (a) distributed and (b) concentrated windings.

machine is assumed to have 12 slots and a convection coefficient of 2000 W/m$^2 \cdot$ K. This is higher than the direct-cooled case because it can use a water-based coolant, but that benefit is limited by additional contact resistance due to the interface with the jacket.

The data presented in Table 1 indicate that for the concentrated and distributed winding configurations, the slot liner starts off as the largest contributor to thermal resistance, but as the rotor diameter increases, the thermal resistance becomes greater in the windings. This transition from dominant to nondominant contributor to thermal resistance happens at roughly the rotor diameters for all three developmental motors specified above. As power required from these machines is only expected to grow, requiring even larger rotors, so will the amount concentration of the thermal resistance in the windings become more dominant.

Based on previous results [9], improvements in the thermal conductivity of insulation materials can be made, including improved effective encapsulation thermal conductivities for Litz wire on the order of 10 W/m $\cdot$ K, and slot liner conductivity of 0.6 W/m $\cdot$ K. The change in scaling behavior is shown in Table 2 for the distributed winding design. The improved materials roughly halve the overall resistance; therefore, the relative percentages of the iron conduction and convection resistance increase, as shown in Table 2. Having improved the materials, the limiting factor becomes the metallic back iron and cooling convection and conduction. This leads to changing the design space to minimize those resistances.

Table 1. Resistance thermal network model results comparing the percentage of total thermal resistance for concentrated and distributed windings utilizing state-of-the-art materials ($K_{\text{slot liner}}$ = 0.1 W/m $\cdot$ K, $K_{\text{effective distributed windings}}$ = 3 W/m $\cdot$ K, $K_{\text{concentrated windings}}$ = 4 W/m $\cdot$ K) [8]

	Rotor diameter (mm)	Winding resistance (%)	Slot liner resistance (%)	Iron conduction resistance (%)	Convection and contact resistance (%)
Concentrated	50	14	62	8	15
	100	23	51	13	13
	200	34	37	19	9
	300	40	30	23	7
	500	47	21	27	5
	700	51	16	29	4
	1000	54	12	31	3
Distributed	50	8	57	5	30
	100	15	51	8	26
	200	24	41	13	21
	300	31	35	17	18
	500	39	26	21	14
	700	44	21	24	11
	1000	49	16	26	8

Table 2. Distributed winding resistance thermal network model results demonstrating the impact of advanced materials ($K_{\text{slot liner}}$= 0.6 W/m $\cdot$ K, $K_{\text{effective distributed windings}}$ = 10 w/m $\cdot$ K) [9]

Rotor diameter (mm)	Winding resistance (%)	Slot liner resistance (%)	Iron conduction resistance (%)	Convection and contact resistance (%)
50	5	24	10	61
100	9	21	17	53
200	15	17	26	42
300	18	14	33	35
500	23	10	41	26
700	25	8	46	21
1000	28	6	50	16

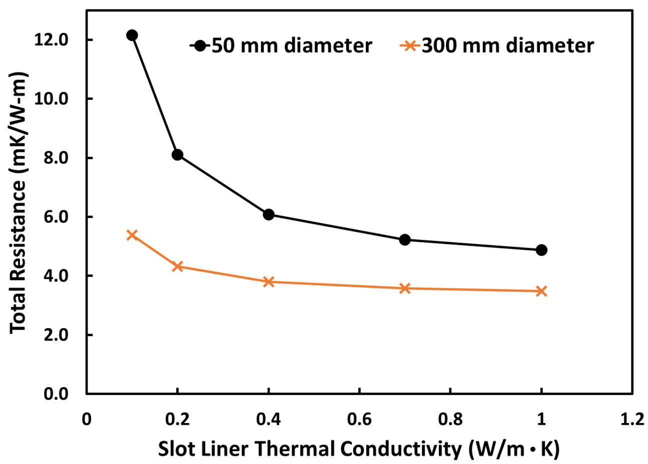

Fig. 3 Total thermal network resistance as a function of slot liner thermal conductivity.

Another way to look at this is to examine the sensitivity of the system to the slot liner. Fig. 3 shows this sensitivity for both the 50-mm and the 300-mm (similar to HEMM) diameter rotor cases. From this example, the impact of rotor diameter is visible. Furthermore, a point of diminishing return is reached at about 0.7 W/m · K. This suggests there is a point where different aspects of the design space will need to be optimized differently.

2. Finite Element and Micromechanical Multiscale Model

At the center of the slot of the distributed-winding high-power-density machines are Litz wire windings. These windings are designed to minimize electromagnetic losses caused by the motor drive frequencies that are necessary to drive high-power-density motors. However, the Litz wire system is complicated by fine wires and layers of electrical insulation and encapsulation. Given that the thermal resistance of the windings eventually becomes the dominant thermal resistance factor for larger motors, it is useful to understand how heat flows through the volume of the windings.

To understand the thermal environment, a multiscale numerical model has been created. The system consists of a highly conductive core (6000 AWG 40 with ~80-µm diameter) with a 4-µm polyimide coating, potted in a two-part high-temperature epoxy. Structural and microstructural composition of the wire is shown in Fig. 4. Previously, a single-scale microthermal analysis [8, 11, 12] was used to estimate thermal fields at the constituent level within the Litz wire system. Although the results revealed useful information at the microscale, there was no communication between the globally applied (macro) loads and resulting local (micro) fields (no communication between micro and macro models). Meanwhile, the macroscopic response of the wire is heavily influenced by the arrangement of the constituents of the wire at the microscale. Hence, a multiscale methodology, enabling a hierarchical, two-way coupled communication between global loads and local fields (communication between micro and macro models), was deemed necessary to study the thermal response of the wire in more detail.

Preliminary features of this material system have been captured in the finite element model (FEM) shown in Fig. 5 [13]. The system consists of four wire bundles (color-coded in different shades of green for better visualization) twisted at ~23° to resemble the true morphology of the wire. Eight-node, first-order coupled thermal/electrical brick elements are utilized to generate a uniform FEM mesh along the wire. A study was also conducted to determine that the mesh density used here produces converged results. For simplicity, material properties for the given system are assumed to be independent of temperature. The sample is then subjected to a transient electrothermal loading step to solve the heat transfer problem under the hypothesis of the presence of the Joule effect as unique source of dissipation (Eq. (1), Table 3).

For consistency with the thermoelectrical experiments conducted at the NASA Glenn Research Center [8], a current as high as ~500 A was applied to the front surface of the specimen (Fig. 5(a)). The top and bottom parts of the specimen are assumed to dissipate heat through convection to the surrounding coolant fluid at a temperature of 60 °C, and the sides were assumed adiabatic. With these boundary conditions, all electrical energy is converted into heat with spontaneous dissipation through convection and radiation (when applicable). During the FEM analysis, the coupled thermal-electrical equation (Eq. (1)) is solved for both temperature and electrical potential at the nodes. It indicates that the power dissipated by joule heating (left side of Eq. (1)) for a given current density value is balanced by convection and radiation heat exchange (right side) where ρ stands for density, S and V are the sample surface and volume of the heat exchange, h and ε are convection coefficient and emissivity respectively, T is the temperature (T_a = ambient temperature/coolant temperature), and σ is the Stefan-Boltzmann constant (5.67×10^{-8} W/m$^2 \cdot$ K^4). More detailed information on electrothermal analysis module is in the FEM software's manual [13].

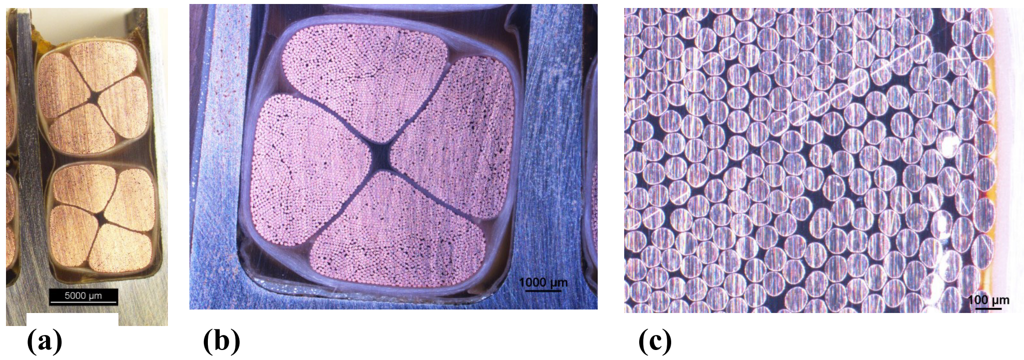

Fig. 4 Optical images of Litz wires. (a) Litz wires configured in stator slot. (b) Closeup of a single Litz wire in a stator slot. (c) Magnified view of individual strands, or microstructure, of a Litz wire.

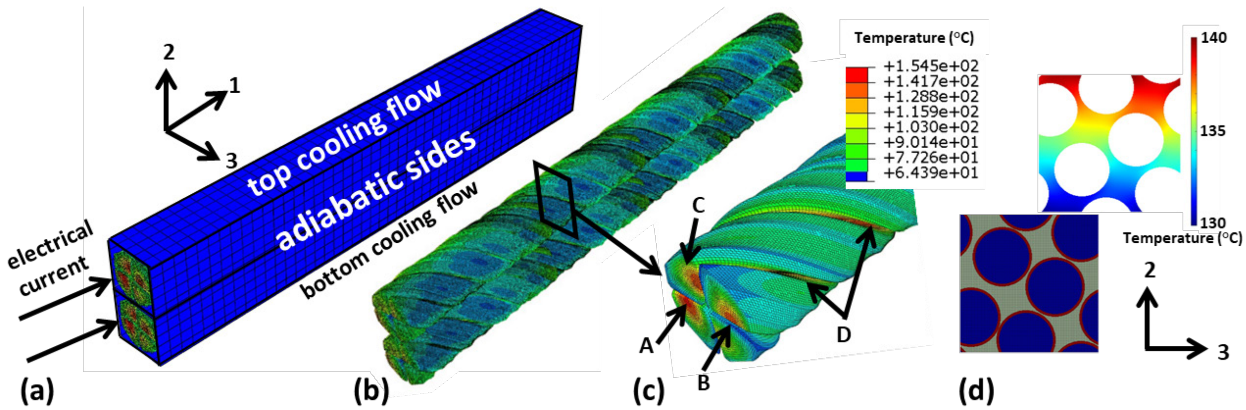

Fig. 5 (a) Sample finite element mesh of a Litz wire stator slot with thermal conditions. (b) Litz wiring showing the twist. (c) Finite element results showing hotspots. (d) Example of a micro-level field RUC that generated micro-level details of the model and the temperature field produced by the model.

$$\rho c\frac{dT}{dt} = \nabla \cdot (\boldsymbol{K}\nabla T) + V|\boldsymbol{R}i^2| + hS(T - T_{ambient}) + \epsilon\sigma(T^4 - T_{ambient}^4)S \tag{1}$$

Table 3. Parameters used with Eq. (1) in the finite element model

Density ρ (kg/m^3)[13]	Specific heat c (J/kg · °C)[13]	Electric resistivity R (μΩ · m) R_1, $R_2 = R_3$[13]	Thermal conductivity (W/m · K) K_1, $K_2 = K_3$ [8]	Convective coefficient (W/m^2 · K)[13]
5500	350	2.8 e-2, 278	238, 1.61	10

Based on the analysis results, the macro-level temperature distribution through the wire bundles seems to be mostly dependent on geometric smoothness and contact surface (Fig. 5(c)). Hotspots (points with temperatures exceeding 150 °C) mostly occur on the front face, where the current is applied, and the bundles come into contact with one another (Fig. 5(c), Regions A-C). However, one can also detect additional hotspots on the surface area of the wire, where there is a directional transition in the twist (Fig. 5(c), Region D). Although the attained maximum temperature in all cases is similar, the directional temperature gradients observed around the hotspots along the twisted surface (Region D) are higher. This information is passed to the micro level (represented by the repeating unit cell (RUC) in Fig. 5(d)).

NASMAT (NASA Multiscale Analysis Tool) is a synergistic multiscale framework that couples the micromechanics directly to the FEM and is capable of modeling advanced composite media [6]. Utilizing NASMAT, one can specify the desired FEM integration points where the high-fidelity generalized method of cells (HFGMC)—a higher-order refined micromechanical theory extended by vector constitutive law—will be called. Global (macro) fields such as temperatures and temperature gradients are passed from the macro level to the RUC, where HFGMC is utilized to calculate the local (micro) fields. Note that HFGMC is tailored toward periodic multiphase media, where periodicity is imposed through continuity of displacements and tractions in an average sense at the surface of the RUC.

As a result, local field distributions (heat flux and temperatures) can be efficiently calculated in a multiphase system [14], striking a balance between simplicity, accuracy, and efficiency. Any given material element point along the wire can be represented by the RUC shown in Fig. 5(d). The conductor core is color-coded as blue, the coating/insulation as red, and the potting material as gray, with constituent properties $K_{\text{conductor}}$ ~400 W/m · K, $K_{\text{coating/insulator}}$ ~0.1 W/m · K, and K_{potting} ~1.3 W/m · K). Using NASMAT, one can investigate the influence of global loads on local fields at desired material points picked in Fig. 5(c), Regions A-C, and in Region D.

When the global (macro) temperature gradients are higher at a certain region (Region D), their influence at the local (micro) level can be nonnegligible. In Regions A-C (Fig. 5(c)), the local temperature observed in the RUC is approximately the same as the global temperature produced by the FEM (~145 °C). However, in Region D (Fig. 5(c)), the local temperature can be approximately 10 °C higher throughout the RUC as compared with the FEM results (~140 °C locally vs. ~130 °C at FEM level). Given that this increase in temperature is not captured in the FEM results and is almost impossible to capture with a temperature measurement device during an experimental measurement, the microscale model has given an important parameter. The maximum operating temperature of a motor, and thus the overall electrical current, is determined by the maximum operating temperature of the electrical insulation. In turn, the maximum operating temperature of the insulation determines the lifetime of the insulation system. The underestimation of temperature of the FEM will need to be considered when determining the operating parameters of an electric machine and thus determining its safe lifetime.

B. Materials

Researchers at the NASA Glenn Research Center have been working on materials that will meet the challenges of enabling high-power-density electric machines for EAP applications. The specific focus has been on the nonmagnetic components, such as slot liners, potting material, wire insulation, and other related structures. The materials under development need to be multifunctional in the sense that not only must they meet requirements such as being electrically insulative, structurally sound, and capable of ~200 °C operation or greater, but they must also enable better thermal management in the stator. The last requirement is particularly important, because the thermal aspects become increasingly difficult as power levels rise. Thermoplastics are the preferred system matrix for this application because of their inexpensive and robust processing. Given that thermoplastics do not exhibit high thermal conductivity, composite systems using boron nitride are of interest. Boron nitride exhibits exceptionally high thermal conductivity (comparable to that of carbon nanotubes) while being electrically insulating and is supplied in various aspect ratios. Furthermore, the system geometries enabled by available thermoplastic processing techniques, such as injection molding and additive manufacturing, could be used to implement complex DWHX concepts.

An example of a high-temperature thermoplastic composite being investigated for EAP applications is polyphenylsulfone (PPSU) embedded with hexagonal boron nitride (hBN) platelets. PPSU is a material of interest for slot liner applications where the service temperature is expected to be approximately 180 °C. This composite is being investigated as a potential slot liner candidate in electric machines due to its high thermo-oxidative stability, toughness, high operation temperature (190 °C), and promising dielectric properties [15, 16]. Recent advancements with the PPSU-hBN composite candidate have provided more understanding about thermal conductivity performance at temperatures approaching the expected operational environment. Other systems being investigated target higher service temperatures while considering cost, mechanical robustness, and dielectric performance relevant to the target application.

Fig. 6 illustrates the temperature-dependent thermal conductivity of pristine PPSU and its composites. The initial room-temperature thermal conductivity of pristine PPSU is ~0.32 W/m·K and increases to ~0.57 W/m·K when closer to the maximum operating temperature. After introducing ~0.6 wt% of boron nitride nanoscale platelets, the thermal conductivity decreased to become lower than the pristine PPSU. Creating a micro-sized (micronized) and hBN mixture creates a unique matrix. The 12.5 wt% PPSU-micronized + nano BN composite (Fig. 6) produced the most promising thermal conductivity results. The results started off at ~0.40 W/m·K at room temperature and increased to an average of ~0.63 W/m·K at 190 °C. The thermal conductivity of the 12.5 wt% PPSU-hBN composite at the maximum operation temperature of 190 °C is near the optimal slot liner thermal conductivity for the stator design prior to displaying the further diminishing returns in motor performance shown in Fig. 3. This advancement removes the slot liner as the main thermal impediment for a HEMM- or UIUC-like machine.

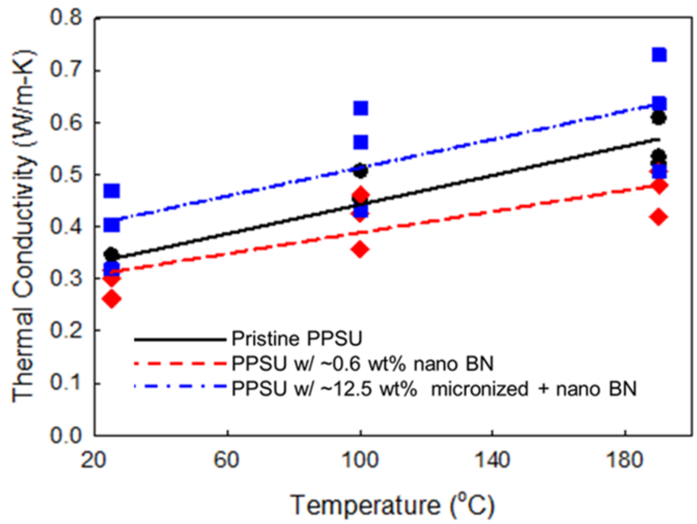

Fig. 6 Temperature-dependent thermal conductivity of pristine polyphenylsulfone (PPSU) and PPSU-boron nitride (micronized and nano) composite films.

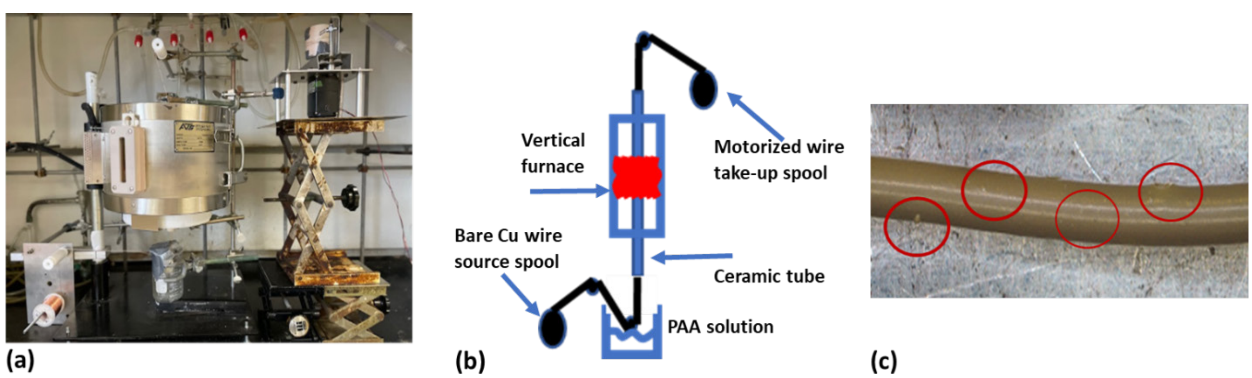

Fig. 7 Polyimide-BNNS coating of Cu wire. (a) Laboratory-scale coating apparatus. (b) Schematic of coating apparatus. (c) Coated, but uncured wire with regions of clumped BNNS (red circles).

Litz wires tend to be the conductor of choice for high-power-density motors due to their ability to suppress several loss mechanisms, such as proximity effects, eddy currents, and skin depth. Litz wire (Fig. 4 and Fig. 8(a)) is made of fine wires (diameters vary depending on drive frequencies and sensitivities to different losses) that are generally coated in polyimide electric insulation with low thermal conductivity. Although the coating is thin, the number of fine, coated wires can be in the thousands, making the coating a significant volume fraction that is distributed throughout the wire bundle system. To that end, increasing the thermal conductivity of that coating is of great interest, and a promising approach has been to create polyimide-boron nitride composites. Previous reports described how boron nitride nanosheets (BNNS) can be used to increase thermal conductivity of polyimide film 5- to 20-fold while maintaining flexibility of the film and having only a mild impact on the dielectric strength of the material [9].

The next step is the coating of a thin wire. Fig. 7 depicts the laboratory-scale coating process; the vertical solvent evaporation furnace apparatus and schematic are shown in Fig. 7(a) and (b), respectively. The vertical furnace is the industry standard for achieving solvent evaporation with a better distribution of polyimide precursor than horizontal evaporation [17]. A 0.81-mm (20 AWG) wire stripped of its layer is exposed to a bath of the polyimide precursor, polyamic acid (PAA), with 34 wt% BNNS using N,N-dimethylacetamide (DMAc) as the precursor. From the source spool, the wire passes through the bath and up through the furnace (180 °C) to the take-up spool. After coating, the wire is transferred to a vacuum oven and cured. Although this preliminary result is encouraging, the existence of visible BNNS clusters (white specks in the red circles) indicates that more work is required to ensure dispersion of the particles in the solution.

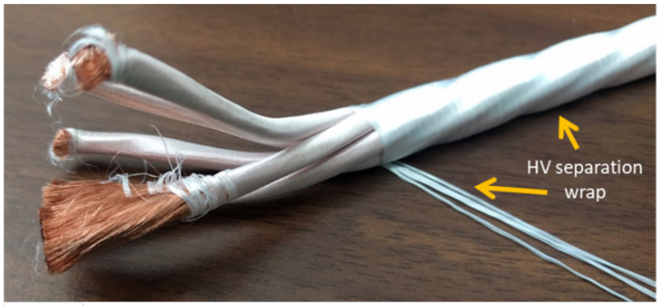

(a)

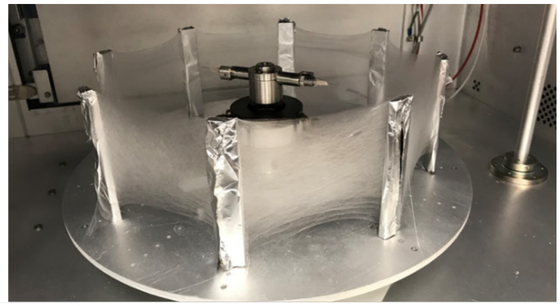
(b)

Fig. 8 (a) Litz wire showing the polyamide HV wrap. (b) Force-spun polymer-boron fibers that can be converted to boron nitride for HV separation applications.

Often Litz wire is wrapped in a polyamide fiber (Fig. 8(a)), which when potted (impregnated and encapsulated) becomes a high-voltage separation material (>3-10 kV for these applications). However, like the other electrically insulating materials in the stator, this material has poor thermal conductivity. To address this, new fibers made of boron nitride are being developed as electrical insulation candidates (Fig. 8(b)). Although the results are preliminary, these fibers are promising candidates to substantially improve thermal conductivity in the wrapping materials.

Processing parameters used in polymer-derived ceramics (PDC) prepared by force spinning (FS) are currently under investigation for the fabrication of hBN nanofibers. The process includes incorporating a boron precursor into a solution with a polymer containing nitrogen, spinning the solution to develop a preform polymeric fiber, curing the fibers, and heat-treating them for ceramic conversion to hBN. The yielded ceramic fibers are expected to have the multifunctional properties of hBN, such as high thermal conductivity, low electrical conductivity, and good mechanical strength along the length of the fiber. The use of FS technology enables the fabrication of fine, continuous fibers that can be collected as nonwoven mats or yarns at a large production rate that can be made into high-thermal-conductivity wrap on the Litz wire.

The polymer polyvinylpyrrolidone (PVP) was chosen from among several polymers considered. PVP has the right viscosity and molecular weight to be combined with the fillers and solvent to create the preform polymeric fibers. PVP has nitrogen in its chemical structure, $[C_6H_9NO]_n$, but preparation of hBN requires the addition of fillers containing boron. The filler used in this research was boron oxide (B_2O_3). Different concentrations of the solutions were tried to create preform polymeric fibers. The polymeric fibers were cured with UV lamps to crosslink the polymer to make the fibers stronger for the heat-treatment conversion to ceramic at high temperature. Temperatures above 1300 °C are needed to achieve the hBN crystalline structure. The gas used during the heat treatment is also key in the synthesis of BN, therefore these samples were heat-treated under nitrogen. Fig. 9 shows the scanning electron micrographs at lower and higher magnifications before (Fig. 9(a-b)) and after (Fig. 9(c-d)) the heat treatment of 1300 °C under nitrogen. After UV crosslinking and after heat treatment, the fibers retained their form with a diameter of around 200 nm. Upon closer inspection of the heat-treated fibers (Fig. 9(c-d)), it can be observed that some fibers are shorter but maintained the fiber structure. Although not depicted in this figure, Fourier transform infrared (FTIR) and x-ray diffraction analysis spectra for the chemical analysis of the different stages of the sample preparation indicate that the PVP/boron oxide solution showed the conversion of the precursors to the desired hBN crystalline structure.

The physical properties of the fibers prepared using FS can be tailored to the needs of the application. The fibers can range from ~200 nm to 5 μm in diameter depending on the precursor properties (e.g., polymer properties, constituents, and solution viscosities) as well as spinning speeds and can be as long as 6 ft in length. A few challenges for the use of the force-spun hBN fibers wrapped on Litz wires need to be addressed. The first challenge is the collection of preform polymeric fibers before the conversion to ceramic. The fiber collection is very similar to a cotton candy machine, where fibers are spun from a spinneret and collected in the collection rods, but for the Litz wire application, a yarn collection attachment is used. This attachment allows preform polymeric fibers to be collected properly and to avoid extra processing to make them a yarn, which could damage the fibers. The second challenge is the ceramic conversion of a preform polymeric fiber yarn into BN fiber yarn. This is due to the continuity of the preform fiber yarn, which will require a new furnace setup for a continuous flow of yarn that needs to be exposed to high temperatures. For this, the heat treatment process will need to be re-optimized for a full conversion to ceramic in a continuous flow. The research is now focused on this application direction.

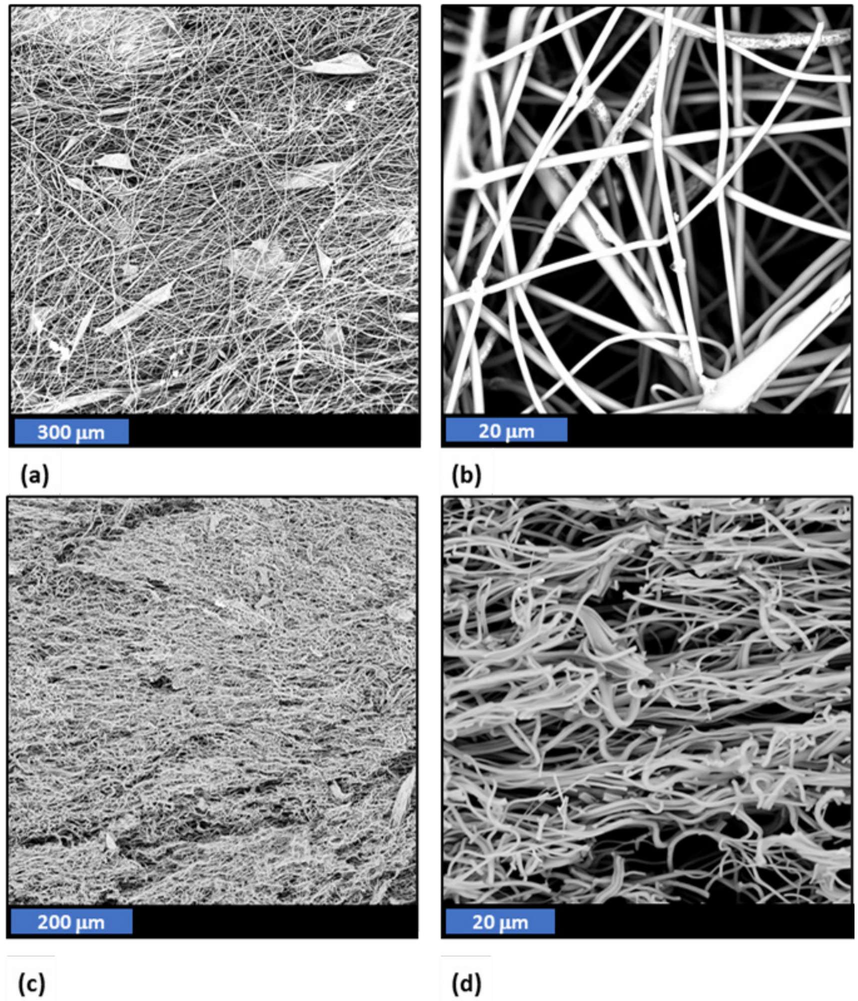

Fig. 9 Scanning electron micrographs of crosslinked force-spun fibers containing PVP and boron oxide, before and after heat treatment at 1300 °C under nitrogen. (a-b) Before heat treatment. (c-d) After heat treatment.

System lifetime is a critical consideration during the material design process. Although materials commonly have aging performance expectations reported, it is well understood that processing conditions can significantly alter aging performance and must be accounted for. Common electrical insulation environmental stresses include thermal, electrical, ambient, and mechanical (TEAM) stressors [18]. Thermal stresses are dominated by the thermal oxidation of polymeric insulators, which leads to embrittlement. Embrittlement significantly reduces the system's resistance to other sources of stress. Electrical stresses include surges and partial discharges (PDs). Ambient stresses result in mild aging but, more importantly, they act synergistically with other TEAM stressors. Examples of ambient stressors include humidity, debris, radiation, and exposure to various chemical compounds associated with system maintenance. Vibration is the primary mechanical stressor, but other mechanical stressors include coefficient of thermal expansion mismatch-induced shear stresses. Researchers at the NASA Glenn Research Center are investigating material systems' performance with consideration of TEAM stressors.

C. Material Impact

While material development and models of the systems are interesting academic pursuits, understanding how they can impact and enable system-level gains is critical to targeting specific enabling applications. The FE modeling indicated that a variety of hotspots develop, not only in the center of the Litz wire but also along the outside of the wire. This indicates the need to boost the thermal conductivity both internally and about the edges. For the hotspots inside the Litz wire, the insulation on the individual strands of Litz wire is one obvious place to gain thermal conductivity, which has been addressed in this paper with the demonstration of the polyimide-BNNS wire coating. Potting processing and materials are another area for improvement. Unfortunately, potting materials with a thermal conductivity of more than 1 W/m · K usually include thermally conductive fillers in an epoxy. When impregnating the wire with the filled epoxy, the fine Litz wire strands and outer wraps act as a filter, keeping the thermally conductive filler on the outside. Therefore, developing the use of nanofiller and accompanying potting techniques that can increase thermal conductivity for those hard-to-reach locations is of great interest [9, 19]. The impact of hotspots on the outside of the bundles will be lessened not only by the polyimide-BNNS and potting improvements but also by more thermally conductive high-voltage separators. This investigation has shown that this can be accomplished with a PPSU-BN extruded slot liner or the BN fiber rap.

Considering the thermal network model, materials advances that are currently underway are removing the insulating and potting materials as thermal roadblocks to higher performance, resulting in longer system life and/or higher power densities. Once these materials are implemented, the major roadblock becomes transfer of heat to the cooling liquid. Unfortunately, the best cooling liquids are not good dielectric liquids, and vice versa [20]. Therefore, direct-winding cooling that utilizes high-performing cooling liquids (e.g., ethylene glycol water mixtures) are of great interest [3]. Thermoplastics with boosted thermal conductivity, such as the PPSU described above, can possibly be injection molded and/or additively manufactured into shapes that can carry fluids closer to the sources of heat and relieve the thermal resistance found in the current back iron and cooling jacket.

IV. Conclusions

Scaling electric machines from hundreds of kilowatts to the megawatt scale is a significant challenge, and stator thermal considerations are a specific concern. As motors scale up for EAP applications, the diameter of the motor increases, and with that, the thermal resistance changes. Specifically, as the diameter of the motor increases, the impact of the slot liner (high-voltage separator) becomes less, and the potting material and wire insulation will have a more significant impact on total thermal resistance. This means that more than one aspect of the machine slot must be addressed to have a significant impact on the thermal environment of the entire machine. The challenges presented here can be addressed through multiple material advancements whereby materials gain multifunctionality.

V. Acknowledgments

This work is primarily sponsored by the NASA Advanced Air Transport Technology Project's Power and Propulsion subproject (Program Manager Amy Jankovsky), with co-funding for the multiscale model from the Transformational Tools and Technology project. Special thanks to Tom Tallerico, Daniel Scheiman, and Brett Bednarcyk.

References

[1] "Sustainable Flight National Partnership." https://www.nasa.gov/aeroresearch/sustainable-aviation-np/

[2] Jansen, R., Bowman, C., and Jankovsky, A., "Sizing power components of an electrically driven tail cone thruster and a range extender," *16th AIAA Aviation Technology, Integration, and Operations Conference*, 2016, p. 3766.

[3] Sixel, W., Liu, M., Nellis, G., and Sarlioglu, B., "Cooling of Windings in Electric Machines via 3-D Printed Heat Exchanger," *IEEE Transactions on Industry Applications*, Vol. 56, No. 5, 2020, pp. 4718-4726. doi: 10.1109/ECCE.2019.8913234

[4] Jansen, R., et al., "High Efficiency Megawatt Motor Preliminary Design," *AIAA Propulsion and Energy 2019 Forum*, 2019, p. 4513.

[5] Yoon, A., Yi, X., Martin, J., Chen, Y., and Haran, K., "A high-speed, high-frequency, air-core PM machine for aircraft application," *2016 IEEE Power and Energy Conference at Illinois (PECI)*, IEEE, Champaign, IL, 2016, pp. 1-4.

[6] Swanke, J. A., Bobba, D., Jahns, T. M., and Sarlioglu, B., "Design of high-speed permanent magnet machine for aerospace propulsion," *2019 AIAA/IEEE Electric Aircraft Technologies Symposium (EATS)*, IEEE, 2019, pp. 1-12.

[7] Sixel, W., Liu, M., Nellis, G., and Sarlioglu, B., "Ceramic 3D printed direct winding heat exchangers for improving electric machine thermal management," *2019 IEEE Energy Conversion Congress and Exposition (ECCE)*, IEEE, Baltimore, MD, 2019, pp. 769-776.

[8] Woodworth, A., Sixel, W. A., Edwards, R., Jansen, R., McCormick, S., Robbie, M., Smith, A., Naghipour, P., and Shin, E. E., "Thermal Analysis of Potted Litz Wire for High Power Density Aerospace Electric Machines," *AIAA Propulsion and Energy 2019 Forum*, Indianapolis, IN, 2019, p. 4509.

[9] Woodworth, A., Williams, T. S., Kelly, M., Sixel, W., Shin, E. E., Nguyen, B. N., and Naghipour, P., "Potential of Materials to Impact Megawatt-Scale Electric Machines," *AIAA Propulsion and Energy 2021 Forum*, 2021, p. 3275.

[10] Simpson, N., Wrobel, R., and Mellor, P. H., "Estimation of equivalent thermal parameters of impregnated electrical windings," *IEEE Transactions on Industry Applications,* Vol. 49, No. 6, 2013, pp. 2505-2515.

[11] Woodworth, A., Jansen, R., Duffy, K. P., Naghipour, P., and Shin, E. E., "Creating a multifunctional composite stator slot material system to enable high power density electric machines for electrified aircraft applications," *2018 AIAA/IEEE Electric Aircraft Technologies Symposium*, Cincinnati, OH, 2018, p. 5012.

[12] Woodworth, A., Smith, A., Jansen, R., and Szpak, G., “Select Variables Affecting Thermal System Design of a Liquid-Cooled Stator,” *AIAA/IEE Electric Aircraft Propulsion Technologies Symposium,* Virtual, 2020.

[13] “ABAQUAS.” Version 6.12-1 ed., Dassault Systémes Simulia Corp., Providence, RI, 2012.

[14] Aboudi, J., Arnold, S. M., and Bednarcyk, B. A. *Mechanics of composite materials: a unified micromechanical approach*: Elsevier, 2013.

[15] Williams, T., Nguyen, B., Woodworth, A., and Kelly, M., “Engineered Interfaces in Extruded Polyphenylsulfone-Boron Nitride Composite Insulation,” *2022 IEEE 4th International Conference on Dielectrics (ICD)*, IEEE, 2022, pp. 94-97.

[16] Williams, T., S, Nguyen, B., and Fuchs, W. K., “Polyphenylsulfone-hBN Composite Insulation,” *IEEE 2020 International Conference on Dielectrics*, IEEE, Valencia, Spain 2020, pp. 541-545.

[17] Rabilloud, G., *High-performance polymers: chemistry and applications*: Editions Technip, 1997.

[18] Panagiotou, P., Lambourne, A., and Jewell, G., “Ex-situ Inspection of Concentrated Stator Coils by Means of Impedance Spectroscopy,” *2022 International Conference on Electrical Machines (ICEM)*, IEEE, 2022, pp. 2331-2337.

[19] Shin, E. E., “Improved potting of Litz Wires for High Power Density Electric Motor,” *AIAA Propulsion and Energy 2021 Forum*, 2021, p. 3292.

[20] Chapman, J. W., Kratz, J. L., Dever, T., Mirhashemi, A., Heersema, N., and Jansen, R., “SUSAN Concept Vehicle Power and Propulsion System Study,” *AIAA SciTech 2023 Forum*, 2023, p. 1749.